Angewandte Chemie
Eine Zeitschrift der Gesellschaft Deutscher Chemiker

Supporting Information

69451 Weinheim, Germany

Bound Cations Significantly Stabilize the Structure of Multiprotein Complexes in the Gas Phase**

*Linjie Han, Suk-Joon Hyung, and Brandon T. Ruotolo**

ange_201109127_sm_miscellaneous_information.pdf

DATA ANALYSIS

All mass spectra were calibrated externally using a solution of cesium iodide (100 mg ml^{-1}) and were processed with Masslynx 4.1 software (Waters, UK). Spectra are shown with minimal smoothing and without background subtraction. The relative abundance of mass-selected tetrameric ions (I_{tet}) was calculated as a percentage of the total intensity of all the signals observed in the mass spectra corresponding to either intact protein complex or its corresponding fragment ions (*i.e.*, monomer or trimer). The relative abundance of the compact form observed for tetrameric ions separated by ion mobility (I_f) was calculated as a percentage of the total intensity of the peaks in the arrival time distribution observed at a selected m/z value corresponding to intact tetramer (or dimer for BLA):

$$I_{tet}\ (\%) = \frac{I_{tet}}{I_{tet}+I_{mon}} \times 100$$

$$I_f\ (\%) = \frac{I_{folded}}{\sum I_{conformers}} \times 100$$

The average relative standard deviation for the determination of either I_{tet} (%) or I_f (%) is 2-4%. The data shown in Figures 1 and 2 include axes labeled in collision energy (units of eV*). The axis is a normalized version of ion kinetic energy, which takes into account both the charge on the ion and reduced mass of the ion-neutral collision complex, for making comparisons across large mass ranges. Although the conversion used here is identical to center-of-mass energy conversion, we do not use this term in this report, as the definition of this quantity has clear implications for ion internal energy and these claims may not extend to the large ions studied here due to the large number of degrees of freedom possessed by protein complex ions. We use the conversion only as a means of normalizing kinetic energies for CIU and CID comparisons across broad mass ranges.

SUPPORTING FIGURES

One example showing peaks with and without cationization

In Figure S1, the mass spectrum of transthyretin (TTR) from solutions containing 100 mM ammonium acetate can be regarded as the peak without cationization (control). The peak become broad to different extents in the presence of different acetate-based salts (2 mM), showing differential degree of cationization. Such broadening is a product of a series of overlapping charge states corresponding to protein complex ions that adhere to different amounts of cations, which cannot be resolved by MS[1]. Also addition of acetate anions with doubly charged cations (Mg^{2+}, Ca^{2+}, Ba^{2+}) results in a slight increase in average charge state values while some of the singly charged alkaline metal cations added (Li^{+}, Na^{+}, K^{+}, Rb^{+}) cause the charge reduction slightly. Therefore, 14^{+} charge state, highlighted in dashed box, was chosen for isolation based on their intensity across each solution state interrogated.

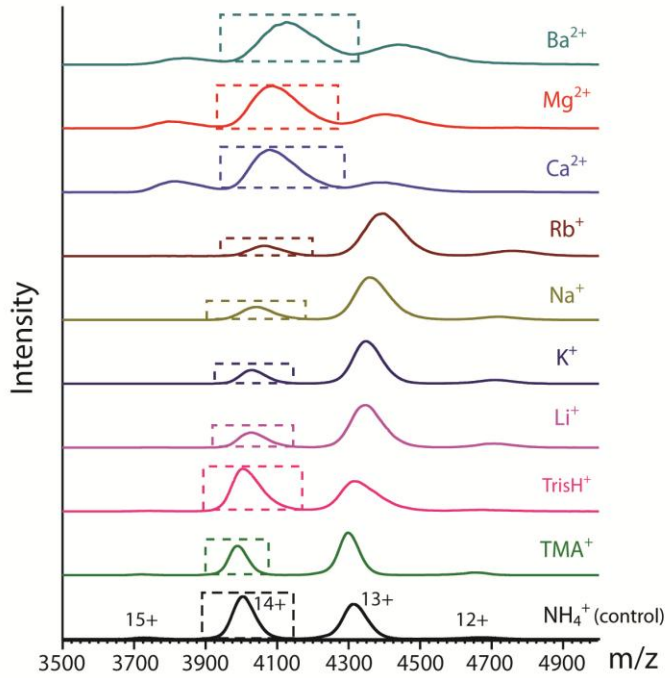

Figure S1. Nanoelectrospray ionization (nESI) mass spectra of tetrameric transthyretin (TTR, 55 kDa) obtained from solution containing 100 mM ammonium acetate (control, black) and a series of solutions containing both 100 mM ammonium acetate and 2 mM salts (acetate anion with tetramethylammonium (TMA), Tris (2-Amino-2-hydroxymethyl-propane-1,3-diol), lithium, potassium, sodium, rubidium, calcium, magnesium, and barium counterions). Each spectrum was obtained using identical instrumental conditions. 14^+ charge state of all TTR-adduct complexes, shown in dashed box, was isolated for CIU/CID.

Details as to the CIU and CID data collected

For quantitative measurement of the differences in the stability conferred to tetrameric protein by bound cations, the trap collision voltage at which ions undergo CID and CIU is monitored, and plots of trap collision voltage versus the intensity observed for intact (I_{tet}) and compact (I_f)

tetramer ions are shown in Figure S2C and Figure S2D respectively. All curves show typical sigmoidal decay. Based on these plots, a simplified descriptor of tetramer stability is constructed by plotting collision energy (units of eV*) at which the intact/compact tetramers (I_{tet} / I_f respectively) decrease to 50% of their initial values (Figure S2E).

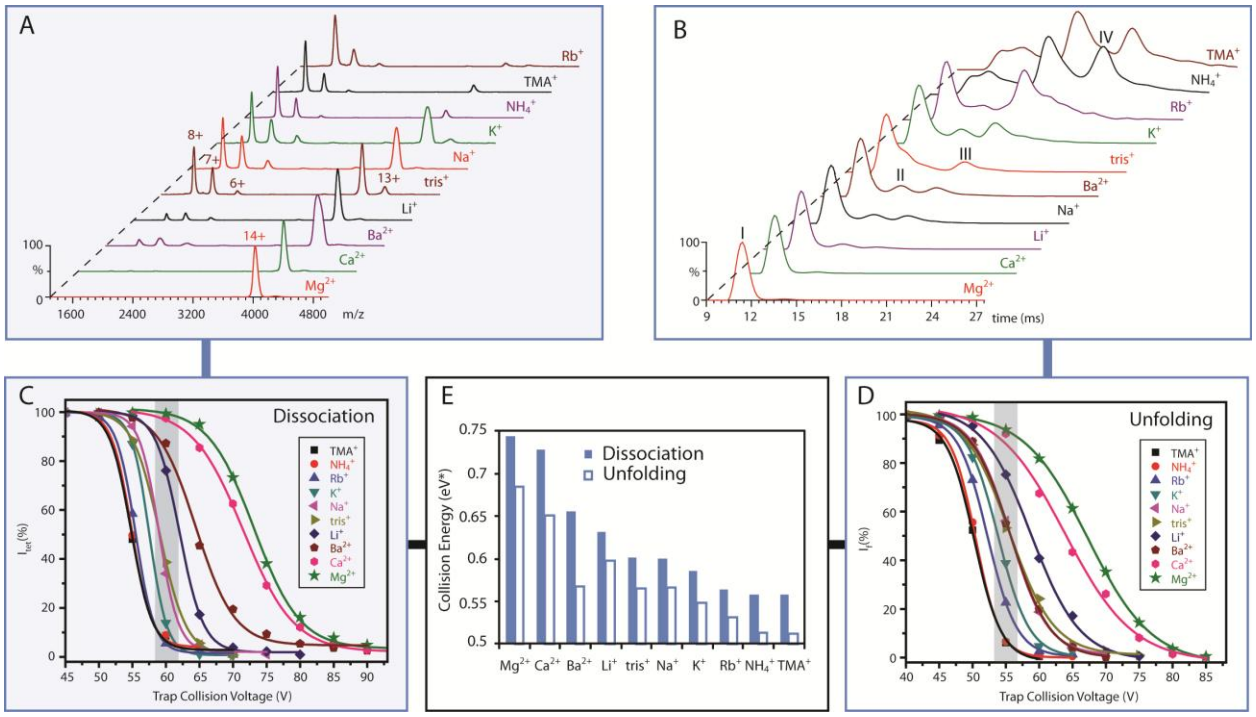

Figure S2. Workflow chart of measuring the stability of cation-bound transthyretin (TTR) by IM-MS. (A) The mass spectra of TTR incubated with 10 acetate-based cations reveal different extent of dissociation. The 14^+ charge state of TTR ions selected by the quadrupole mass filter, acquired at a trap collision voltage of 60 V which was applied to the ions in the trapping region between the quadrupole mass analyzer and ion-mobility region of the instrument. Peaks corresponding to 14^+ charge states of tetramer and $6–8^+$ charge states of monomer are shown. (B) The arrival time distributions of 14^+ TTR incubated with 10 acetate-based cations acquired at a trap collision voltage of 55 V yield unfolding to different extent. The four conformations showing a transition from compact to extended species are labeled from I to IV. (C) Plots of the

relative intensities of intact TTR tetramer 14^+ ions generated with solutions containing 10 different cations (I_{tet}) are shown as a function of trap collision voltage. I_{tet} acquired at a trap collision voltage of 60 V are marked in a grey box. (D) Plots of the relative intensity of compact TTR tetramer 14^+ ions (I_f) are shown as a function of trap collision voltage. I_f acquired at a trap collision voltage of 55 V are marked in a grey box. (E) A histogram showing the 50% dissociation yield (blue) and unfolding yield (white) for TTR tetramers generated from solutions with various cation additives is shown.

Detailed data regarding ADH dissociation

In Figure S3, the relative intensity of intact ADH tetramer ions incubated with Mg^{2+} is still high at the maximum value the trap collision voltage can go (200 V), with different TRAP DC bias tuned. This indicates that ADH-Mg complex does not appreciably undergo CID even at the highest activation energy, which makes it impossible to plot the complete sigmoidal decay curve of I_{tet} as a function of trap collision voltage as shown in Figure S2C.

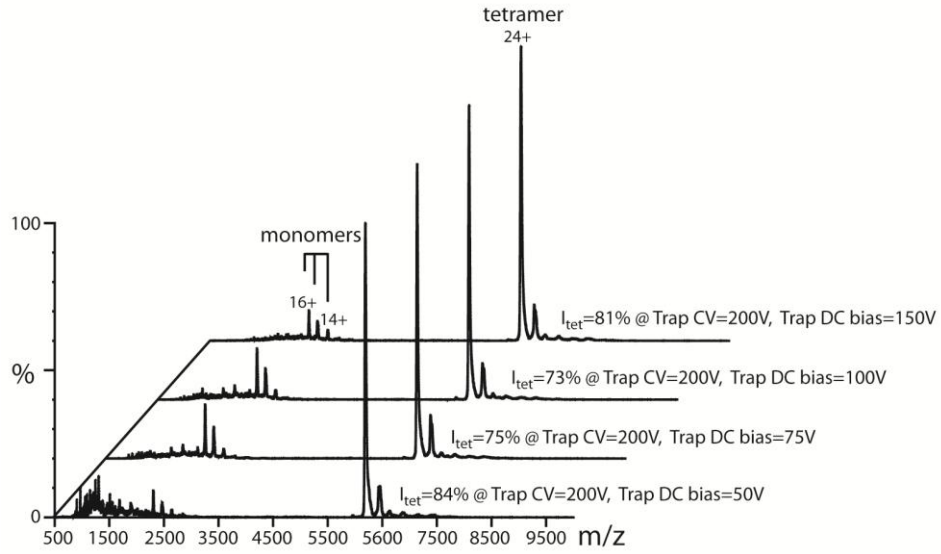

Figure S3. Tandem mass spectra of 24^+ charge state of alcohol dehydrogenase (ADH) incubated with magnesium cations at the maximum accelerating potential difference attainable by Synapt G2 instrumentation (200 V), with different Trap DC bias set, all results in high I_{tet}.

Further observations revealing the potential difference in stabilization mechanism provided by cationic and anionic additives

Learning from our previous study which implied a role for bound anions in observed stability enhancement[2], we probed the number of bound cation additives, carried with the complex from solution or the nESI process by measuring the mass of the protein complexes incubated with the acetate-based cations under identical instrument conditions (Trap CV=4 V). Based on the assumption that the excess mass, relative to the ammonium acetate control arises from binding of additional cations added in solution, we plotted the estimated average number of additional cations bound to the tetramers at the very low activation energy against the stability enhancement observed in our CIU data. This is shown in Figure S4, where singly and multiply charged cations are grouped separately with different colors (2^+: black squares; 1^+: red circles; $TrisH^+$ is excluded). The two groups indicate a strong positive correlation between the amount of excess mass and structural stability conferred to the four tetrameric protein assemblies studied here, implying that the bound buffer material is an important factor behind the added stability to the proteins. However, Mg^{2+} and Ca^{2+}, which are considered to be strong stabilizers, bind in smaller numbers to the protein complexes at the initial voltage than Li^+ that lies in the medium-stabilizing cluster. This is different from that is observed for anion stabilizer which exhibited an "dissociative cooling" type mechanism, featuring a higher structure stabilization effect provided

by greater number of anions bound first and dissociated upon collisional activation[1]. Therefore, this clear charge dependence reveals a potentially different stabilization mechanism that relies on the chemical nature of cationsAlso worth noting is $TrisH^+$ (purple triangle), which acts as an outlier relative to other cations. It affords slight structural stabilization effect to TTR and avidin equally to Na^+ because of its little binding at the low acceleration voltage (Figure S4A/S4B). Conversely, some of $TrisH^+$ cations are observed to bind to ConA and ADH, resulting in a higher stability increase, approaching or even above Li^+ (Figure S4C/S4D).

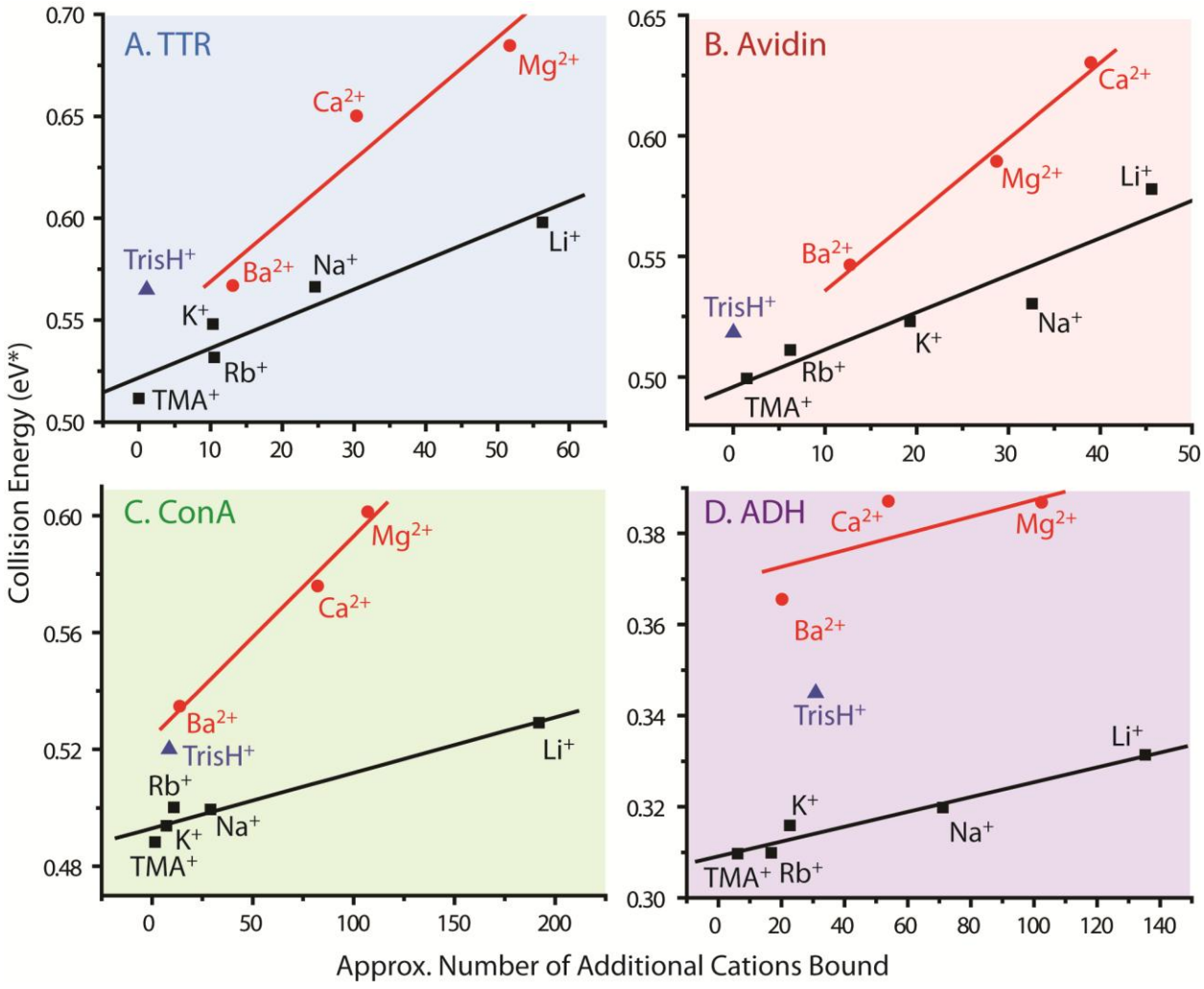

Figure S4. Plots of the normalized collision energy required to unfold 50% of complex ions against the calculated number of additional cations that are bound to the protein complex at a trap collision voltage of 4 V, for transthyretin (A), avidin (B), concanavalin A (C), and alcohol dehydrogenase (D). A positive correlation is observed for all complexes when doubly and singly charged cations (except $TrisH^+$) are treated separately. All lines are added to guide the eye, and are not intended to be theoretical fits to the data presented.

Charge-per-unit-area as an important factor for different mode of stabilization

As illustrated in Figure 2C in the main text, the stability conferred to the gas-phase assembly increases with the charge-per-unit-area of all cations but $TrisH^+$. This is shown more clearly in Figure S5A, which displays a perfect correlation between the charge-per-unit-area of the cations and their ability to stabilize the protein complexes from unfolding in the gas phase (R^2=0.954), with $TrisH^+$ excluded. Cations of higher charge-per-unit-area, such as Mg^{2+} and Ca^{2+}, which bind in large numbers to protein complexes, will retain their binding position within the protein sequence and become less mobile as charge carriers. This reduction in charge mobility and possibly lower conformational flexibility through multidentate binding of cations to sites on the protein hinder Coulomibic unfolding of protein subunits [3]. On the other side, cations of low charge-per-unit-area, that scales in line with the anions studied previously (Figure S5B), does not display an appreciable stabilizing effect mentioned above, resulting from the weakness to lock down charge carriers and tether together multiple sites within proteins (not including $TrisH^+$). Instead, dissociative cooling becomes the dominant effect, equivalent to their anionic counterparts. A low charge-dense cation as $TrisH^+$ is, it exhibits a medium-range stabilizing

influence on gas-phase protein structure, thus suggesting its potential for H-bonding and more-directed interactions with the protein surface on top of the electrostatic interaction.

For exact values of charge-per-unit-area, see Table S1.

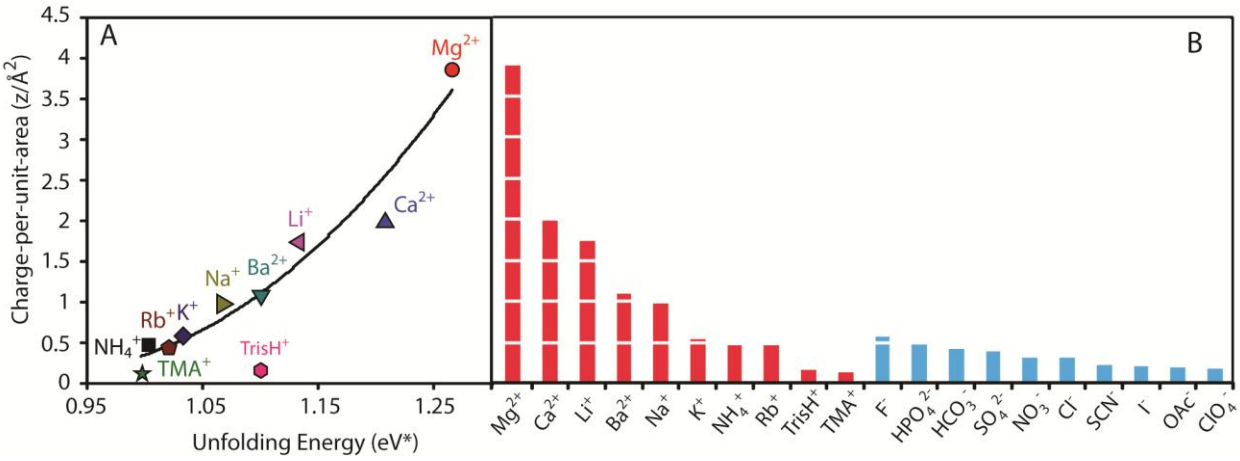

Figure S5. (A) The plot extracted from Figure 2C clearly shows an excellent correlation between the charge-per-unit-area of the cations and the stabilization observed for the proteins studied here (R^2=0.954) only when $TrisH^+$ is excluded. (B) Charge-per-unit-area of the cations (red) and anions (blue) studied shows cations in general possess significantly higher charge per-unit area compared to anions.

SUPPORTING TABLE

Table S1. Physical constants of selected Hofmeister cations and anions including charge, ionic radii and charge-per-unit-area

Cation	Charge	Ionic Radii (Å)	Charge Per-unit-area ($z/Å^2$)
Mg^{2+}	2	0.72	3.858025
Ca^{2+}	2	1	2
Li^{+}	1	0.76	1.731302
Ba^{2+}	2	1.36	1.081315
Na^{+}	1	1.02	0.961169
K^{+}	1	1.38	0.5251
NH_4^{+}	1	1.48	0.456538
Rb^{+}	1	1.49	0.45043
$TrisH^{+}$	1	2.55[a]	0.153787
TMA^{+}	1	2.8	0.127551
Anion	**Charge**	**Ionic Radii (Å)**	**Charge Per-unit-area ($z/Å^2$)**
F^{-}	1	1.33	0.565323
HPO_4^{2-}	2	2	0.5
HCO_3^{-}	1	1.56	0.410914
SO_4^{2-}	2	2.3	0.378072
NO_3^{-}	1	1.79	0.3121
Cl^{-}	1	1.81	0.305241
SCN^{-}	1	2.13	0.220415
I^{-}	1	2.2	0.206612
OAc^{-}	1	2.32	0.185791
ClO_4^{-}	1	2.4	0.173611

a. K. Nakashima, S. Tuboi, J. Biol. Chem. **1976**, 251, 4315-21.
Other ionic radius were obtained from Ion Properties (Yizhak Marcus).

References

1. A. R. McKay , B. T. Ruotolo , L. L. Ilag , C. V. Robinson , *J. Am. Chem. Soc.* **2006**, 128, 11433-11442.

2. L. Han, S. J. Hyung, J. J. S. Mayers, B. T. Ruotolo, *J. Am. Chem. Soc.* **2011**, *133*, 11358-11367.

3. a) J. C. Jurchen, E. R. Williams, *J. Am. Chem. Soc.* **2003**, *125*, 2817-2826; b) I. Sinelnikov, E. N. Kitova, J. S. Klassen, *Journal of The American Society for Mass Spectrometry* **2007**, *18*, 617-631; c) S. V. Sciuto, J. Liu, L. Konermann, *Journal of The American Society for Mass Spectrometry* **2011**, 22, 1679-1689; d) S. N. Wanasundara, M. Thachuk, *J. Phys. Chem. A* **2009**, 113, 3814-3821.